p53 induces skin aging by depleting Blimp1^{+} sebaceous gland cells

J Kim[1], M Nakasaki[2], D Todorova[1], B Lake[1], C-Y Yuan[1], C Jamora[2] and Y Xu*,[1]

p53 is an important inducer of organismal aging. However, its roles in the aging of skin remain unclear. Here we show that mice with chronic activation of p53 develop an aging phenotype in the skin associated with a reduction of subcutaneous fat and loss of sebaceous gland (SG). The reduction in the fat layer may result from the decrease of mammalian TOR complex 1 (mTORC1) activity accompanied by elevated expression of energy expenditure genes, and possibly as compensatory effects, leading to the elevation of peroxisome proliferator-activated receptor (PPAR)γ, an inducer of sebocyte differentiation. In addition, Blimp1^{+} sebocytes become depleted concomitantly with an increase in cellular senescence, which can be reversed by PPARγ antagonist (BADGE) treatment. Therefore, our results indicate that p53-mediated aging of the skin involves not only thinning through the loss of subdermal fat, but also xerosis or drying of the skin through declining sebaceous gland activity.
Cell Death and Disease (2014) **5**, e1141; doi:10.1038/cddis.2014.87; published online 27 March 2014
Subject Category: Cancer Metabolism

In mammals, the skin is the largest organ comprising of multiple layers needed to protect the body from a variety of insults reaching the interior. To maintain this function under various stress conditions, the skin and its appendages must be dynamically replenished by local stem cell pools. As the skin consists of several cell types including keratinocytes, adipocytes, sebocytes, and fibroblasts, it is important to understand how the functional interaction among these cell types maintains the health and activity of this organ.

We previously reported that depletion of adult stem cells residing in different organs displayed aging-associated phenotypes,[1] and expected that skin aging also correlates with the state of local stem cells pools in the skin. Recently, a skin-specific p53 activation mouse model, generated by conditionally deleting Mdm2, showed gradual thinning of the epidermis and loss of hair follicle stem cells (HFSCs), resulting in delayed wound healing and loss of hair.[2] However, this morphology differs from aged skin that additionally becomes thinner in the dermis,[3] a phenotype already reported for p53-mediated accelerated aging by the same group.[4] These results suggest that skin aging phenotypes arise from defects in multiple cell types and not simply the epidermal derivatives. In fact, HFSCs residing within the bulge is regulated by dermal cells such as adipocytes, dermal papilla

(DP) cells, and fibroblasts.[5,6] However, how these cell types are coordinated with other stem cells/progenitor cells during aging remains unclear.

Dry skin (xerosis) is a common appearance in the elderly and its incidence and severity increase with age. But, the cause of dry skin has been controversial, as it is attributed to multiplefactors, including cellular turnover, lipid content, activity of glands, hydration, skin barrier function, and transepidermal water loss.[3] In spite of this confusion, there is no question that skin oiliness and moisture, which correlate to lipids and water contents, respectively, are involved in dry skin. Sebaceous gland (SG) contributes to both the factors by delivering a complex lipid mixture, sebum, to the skin surface and regulating stratum corneum (SC) hydration.[7] Homeostasis of SG is maintained by constant replenishment of sebocytes differentiated from either the Blimp1-expressing sebocyte progenitor cells or diverse stem cells in the bulge.[8] This differentiation is regulated by several signaling pathways such as Wnt, Hedgehog, and lipid metabolism. Notably, the SG activity is decreased in aged skin with the reduction of sebum; however, the decline is correlated to sex.[9] Although it has been known that SG differentiation and SG progenitor cells are affected by aging,[10–13] it remains to be elucidated how aging depletes SG progenitor cells. Interestingly, the mouse with the disruption of stearoyl-CoA desaturase

(SCD)1, which is the critical enzyme for fatty acid synthesis, displayed atrophy of SG.[14] This suggests that there is a close relationship between the decrease of SG activity with age and the reduction of subcutaneous fat with aging.

While previous studies clearly ascribe a potential role for active p53 in skin aging, the underlying mechanism has yet to be fully understood, especially considering the complex roles of Mdm2 in p53-independent pathways.[15] To address this, we examined the skin of $p53^{TSD/-}$ mice with two phosphomimetic mutations (T21D and S23D) introduced into the endogenous p53 gene.[1] The mutations of these residues within the Mdm2/MdmX binding region, which are normally phosphorylated downstream of DNA damage, result in constitutive p53 activation. We have previously shown that these mice exhibit aging-like phenotypes in many systems such as hematopoiesis, reproductive, and digestive systems. These systems can be rescued by depleting the p53 target apoptotic gene *Puma*, indicating critical roles of p53-dependent apoptosis in aging of these tissues.[1,4] In this report, we demonstrate that p53 has multiple roles in the aging of the skin by depleting the skin of vital fat and rejuvenating sebaceous secretions.

Results

$p53^{TSD/-}$ mice show senescence in the SG but not apoptosis.

It has been previously shown that $p53^{TSD/-}$ mice have a diminution of adult stem cells in diverse tissues such as bone marrow, brain, and testes.[1] It is expected that $p53^{TSD/-}$ mice could exhibit a reduction of adult stem cells in the skin like other organs.[16] To check this expectation, skin of $p53^{TSD/-}$ was analyzed. The most obvious skin phenotype in the $p53^{TSD/-}$ mice is a hyperpigmentation of the footpad and tail (Figure 1a), consistent with a previously ascribed role for p53 in melanocytosis following DNA damage or translational stress.[17] Thus, this observation supports the p53 activation in the skin of $p53^{TSD/-}$ mice.

As the depletion of various adult stem cells and its relative aging phenotypes were attributed to apoptosis by p53 activation,[1] we checked whether apoptosis was induced in the skin of 3-week-old or 4-week-old $p53^{TSD/-}$ mice. Apoptotic markers in the skin of $p53^{TSD/-}$ mice remained unchanged, including the expression of *Puma*, which is critical for apoptotic stem cell depletion in other organs (Figures 1b and c and Supplementary Figure S1a). In contrast to a previous report that showed depletion of HFSC in the skin of
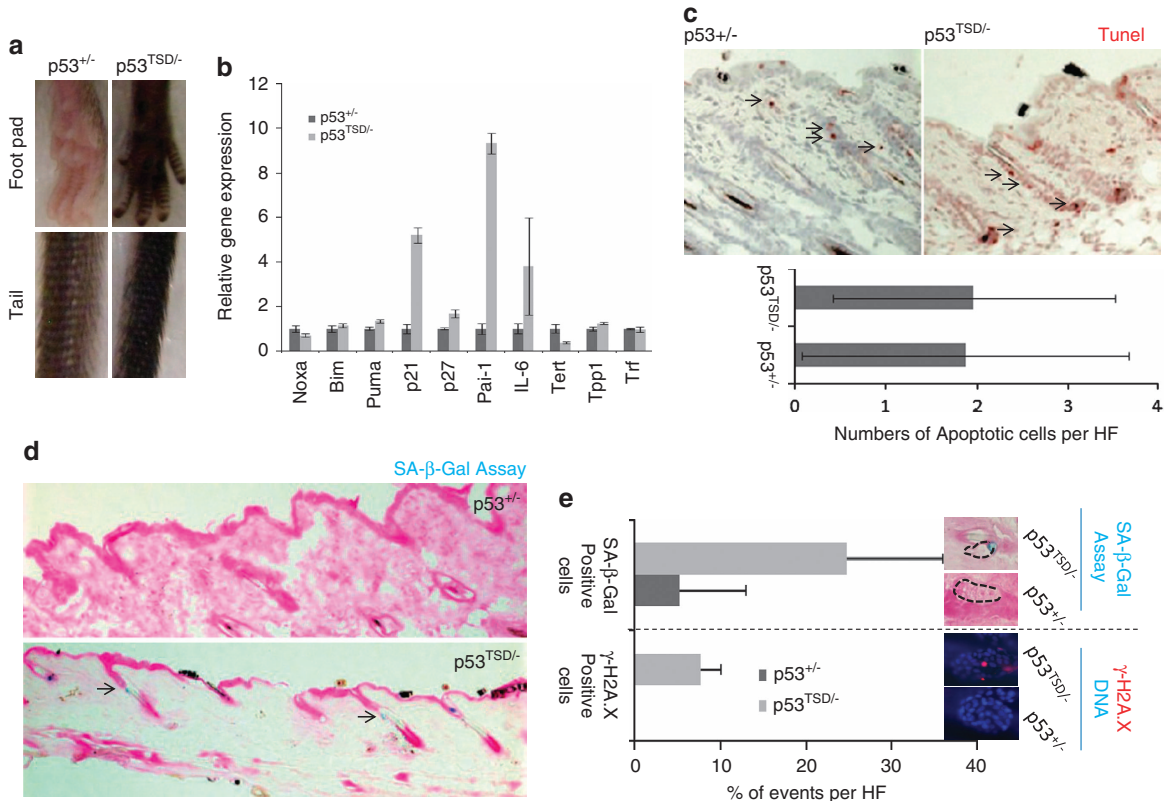

Figure 1 Skin of $p53^{TSD/-}$ mice reveals senescence with p53 activation but not apoptosis. (**a**) Skin of $p53^{TSD/-}$ mice display hyperpigmentation. Macroscopic appearance of tails and foot pads of 4-week-old $p53^{+/-}$ and $p53^{TSD/-}$ mice. (**b**) The relative expression of genes related to apoptosis such as *Noxa*, *Puma*, and *Bim*, as well as genes related to senescence in the skin of $p53^{+/-}$ and $p53^{TSD/-}$ mice was determined by quantitative RT-PCR analysis. The mRNA levels of the senescence-related genes *p21*, *p27*, *Pai1*, and *Tert1* are increased in the skin of $p53^{TSD/-}$ mice, compared with those in $p53^{+/-}$ mice. $n = 3$. Values represent means ± S.D. (**c**) The apoptotic cells were identified by TUNEL assay. Number of apoptotic cells per hair follicle in 4-week-old $p53^{+/-}$ and $p53^{TSD/-}$ mice was counted. $n = 30$–35 HF for each genotype. Values represent means ± S.D. (Magnification, × 50). (**d**) SA-β-gal staining in the skin of $p53^{+/-}$ and $p53^{TSD/-}$ mice (Magnification, × 50). (**e**) Quantification of hair follicles showing SA-β-gal activity and DNA damage foci and in the skin of $p53^{+/-}$ and $p53^{TSD/-}$ mice. Epidermal sheets of $p53^{+/-}$ and $p53^{TSD/-}$ mice were labeled for γ-H2A.X (red) as a senescent marker by immunofluorescence (IF) and representative images of sebaceous gland (SG) are shown. Quantification (the % of cells with DNA damage foci or SA-β-gal activity within SG) was shown in each panel. $n = 3$–4 fields from two mice for each genotype. Values represent means ± S.D. (Magnification, × 100)

p53-activated mice was due to the disruption of Mdm2/p53 interaction,[2] data showed that the HFSC within the bulge failed to show a significant change compared with $p53^{+/-}$ controls (Supplementary Figure S1b). That might be explained by the results of apoptosis not being activated in the skin of $p53^{TSD/-}$ mice. However, these results do not exclude the possibility of more long-term defects that would likely be observed if further aging was possible, similar to prior reports.[4]

In contrast to apoptosis, we observed elevated senescence in the whole skin of $p53^{TSD/-}$ mice through FACS analyses (Supplementary Figure S1c) and elevated expression of senescence-related genes *p21*, *p27*, plasminogen activator inhibitor1 (Pai1), and the decrease of telomerase reverse transcriptase 1 (Tert1) (Figure 1b). In further support of this conclusion, the expression of pro-senescence genes promyelocytic leukemia (*PML*) and *p16* was also increased (Figures 6c–e), while the levels of proliferative marker Ki-67 were decreased in the skin of $p53^{TSD/-}$ mice (Supplementary Figure S1d).

To determine the cellular origin of this senescence, we used cytochemical senescence-associated β-galactosidase (SA-β-gal) analysis and found more positive staining in the hair follicles in $p53^{TSD/-}$ mice than in $p53^{+/-}$ mice (Figure 1e). Interestingly, the staining was localized to the sebaceous gland (Figure 1d). As a reliable indicator of *in vivo* senescence,[18] DNA damage foci defined by phosphorylated H2A.X (γ-H2A.X) was increased in the whole mount of epidermal sheets including SG from $p53^{TSD/-}$ mice (Figure 1e). While the bulge spontaneously showed DNA damage foci even in the $p53^{+/-}$ mice, DNA damage foci in the SG was only evident in $p53^{TSD/-}$ mice.

$p53^{TSD/-}$ mice show a dramatic reduction in subcutaneous fat. The skin of $p53^{TSD/-}$ mice displayed characteristics of aging skin, such as the reduction of dermal thickness and subcutaneous fat (Figure 2a). While the skin thickness in $p53^{TSD/-}$ mice was similar to that in $p53^{+/-}$ mice at P22, the skin thickness in $p53^{TSD/-}$ mice became reduced at P28 (Figure 2b, Supplementary Figures S2a and S2b). In contrast to the dermis, the epidermal thickness was not changed, accompanied by normal staining of epidermal differentiation markers (Supplementary Figure S3). As the small adipocytes were prevailing in the skin of P28-old $p53^{TSD/-}$ mice in contrast to P28-old $p53^{+/-}$ mice, the reduction of adipose tissue in the skin of $p53^{TSD/-}$ mice was likely attributed to the decreased size of adipocytes (Figure 2c). The reduced adipocytes in the skin of $p53^{TSD/-}$ mice is not due to the decrease in the food uptake because $p53^{+/-}$ and $p53^{TSD/-}$ mice consumed a similar amount of food (Figure 2d). To support the notion that the defects in the subcutaneous fat layer are intrinsic but not secondary to the systemic defects, the skin of $p53^{TSD/-}$ and $p53^{+/-}$ mice was transplanted onto the back of SCID mice, showing reduced adipose tissue in the transplanted skin of $p53^{TSD/-}$ mice when compared with that of $p53^{+/-}$ mice (Figure 2e). Together, these data indicate that the reduction of subcutaneous fat layer in the $p53^{TSD/-}$ mice is likely due to p53 activation.

mTOR pathway is involved in modulating the size of adipocytes, and disruption of this pathway and its proteins, such as the regulatory-associated protein of mTOR (Raptor) and 4E-binding protein (4EBP)1, an effector of mTORC1, leads to lean mice with the reduction of adipose tissue through energy expenditure.[19,20] As it has also been reported that p53 inhibits mTORC1,[21] and transcriptional activity of p53 is increased in the subcutaneous fat layer of $p53^{TSD/-}$ mice (Supplementary Figure S4), the reduction of adipose tissue in the skin of $p53^{TSD/-}$ mice could be due to the inhibitory effect of p53 on mTORC1. Consistent with these reports, the phosphorylation of 4E-binding protein (4EBP)1, a substrate of mTORC1 in subcutaneous adipose, was declined in the skin of $p53^{TSD/-}$ mice, particularly in the dermis and fat layer (Figures 3a and b). In addition, the phosphorylation of ribosomal protein S6 kinase (S6K), another mTOR effector, was decreased in the skin of $p53^{TSD/-}$ mice (Figure 3b), and the energy expenditure genes such as uncoupling protein (Ucp)s and *PGC-1α* were upregulated in the skin of $p53^{TSD/-}$ mice particularly the dermis/fat layer (Figures 3c–f). Because the elevated expression of *PGC-1α* and *Ucp1* are normally restricted to brown fat cells, we in the skin of $p53^{TSD/-}$ mice checked the Brown-Beige-restricted genes such as *PR Domain Zinc Finger Protein 16* (*Prdm16*) and *cytochrome c oxidase subunit VIIIb* (*Cox8b*) that are expressed in beige adipocyte located in the subcutaneous fat layer.[22] Both genes are highly upregulated in $p53^{TSD/-}$ mice, suggesting abnormal adipocyte composition in the skin of $p53^{TSD/-}$ mice (Supplementary Figure S6).

A similar reduction of subcutaneous fat was also observed following food deprivation, implying metabolic stress, a physiological inhibitory condition of mTORC1 activity (Figures 3j and k and Supplementary Figure S5). Furthermore, thinning of intradermal adipose tissue was also seen in the skin of $p53^{TSD/-}$ mice injected either with a mTORC1 inhibitor rapamycin (Rapa) or a mitochondrial uncoupler 2,4-dinitrophenol (DNP) (Figures 3g and i and Supplementary Figure S5). In contrast to this, cyclosporin A (CSA) that reduces mitochondrial uncoupling, partially rescued the reduction of subcutaneous adipose in the $p53^{+/-}$ mice (Figure 3h and Supplementary Figure S5). These results suggest that the decrease of the subcutaneous adipose in the skin of $p53^{TSD/-}$ mice is attributed to the downregulation of mTORC1 activity.

Consistent with the previous report that adipocytes regulate the hair follicle cycle,[23] the reduction of adipose may affect the hair follicle cycle as shown in the skin of P28-old $p53^{TSD/-}$ mice (Figure 2a). While in the skin of $p53^{+/-}$ mice, hair follicle cycles were normal from the resting phase (telogen; P22) to the activation phase (anagen; P28), the cycles were delayed in the skin of $p53^{TSD/-}$ mice. As $p53^{TSD/-}$ mice did not survive after 4 weeks, we could not conclude whether the delayed hair follicle cycle is permanent or not. Therefore, we used a *Puma*-null background that rescued the early death of $p53^{TSD/-}$ mice.[1] Notably, we observed hair follicles in the anagen in the skin of $p53^{TSD/-}$ *Puma*$^{-/-}$ mice after 4 weeks (Figure 4e). Moreover, the skin of $p53^{TSD/-}$ *Puma*$^{-/-}$ mice displayed increased p53 activity, but there was normal wound healing in a *Puma*-null background (Figures 4a–c) and normal hair re-growth after shaving (Figure 4d). These results suggested that the hair cycle in the skin of $p53^{TSD/-}$ mice is delayed but is not permanently defective.
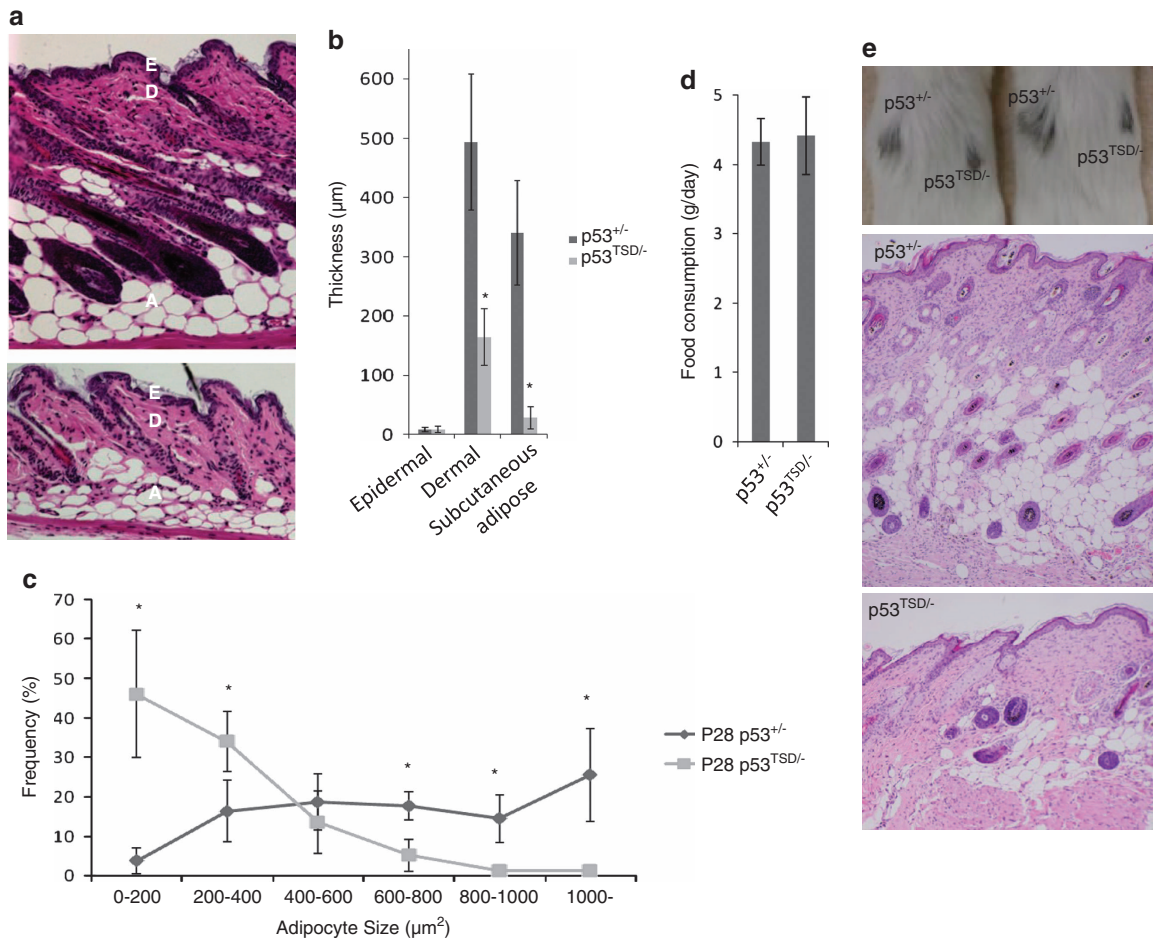
Figure 2 Skin of $p53^{TSD/-}$ mice exhibits the reduction of subcutaneous adipose tissue. (**a**) Hematoxylin-eosin (H&E) analyses of the skin of the $p53^{TSD/-}$ and $p53^{+/-}$ mice at P28 reveal the reduced subcutaneous adipose tissue. A, adipose tissue; E, epidermis; D, dermis. Magnification, ×50. (**b**) The thickness of dermis, epidermis, and subcutaneous adipose tissue of H&E-stained skin sections of the $p53^{TSD/-}$ and control $p53^{+/-}$ mice was measured with the measurement tool in ImageJ. Mean values from four mice for each genotype were presented with S.D. t-test was used to calculate the statistical significance. (**c**) Size of the subcutaneous adipocytes in H&E-stained skin sections of the $p53^{TSD/-}$ and control $p53^{+/-}$ mice was determined with the measurement tool in ImageJ. Mean values from four mice (>100 cells per mouse) for each genotype were presented with S.D. *$P < 0.05$. (**d**) Food consumption of $p53^{TSD/-}$ mice and $p53^{+/-}$ mice. Three-week-old mice were monitored for 1 week. $n = 3$. (**e**) Reduced adipose tissue in the skin of $p53^{TSD/-}$ mice grafted onto the back of the same SCID mouse. The skin of $p53^{TSD/-}$ and control $p53^{+/-}$ mice were grafted onto the back of the same SCID mouse for four weeks and analyzed by H&E staining. The skin grafts were derived from newborn mice. The upper panel shows the image of skin grafts on the back of SCID mice. The middle and bottom images show the H&E-stained sections of the skin grafts in the same scale

p53-dependent senescence is correlated to the depletion of SG progenitors and ROS. Given the data of the decreased size of adipocytes in the skin of $p53^{TSD/-}$ mice and the induction of senescence in the SG, we considered the relationship between subcutaneous adipocytes and sebocytes in the skin. Both sebocytes and adipocytes are the cells that accumulate lipid droplets and utilize the transcription factor peroxisome proliferator-activated receptor γ(PPARγ) in their differentiation programs.[24–26] Therefore, we checked whether PPARγ and its target genes involved in adipogenesis were changed in the skin of $p53^{TSD/-}$ mice. Interestingly, there was upregulation of lipogenic genes such as *Acetyl-coA carboxylase* (*ACC*), *Fatty acid synthase* (*FAS*), *Stearoyl-CoA desaturase1* (*Scd1*), and *Sterol regulatory element-binding protein1* (*Srebp1*) in the skin of $p53^{TSD/-}$ mice, as well as the induction of *PPARγ* and glucose *transporter4* (*Glut4*), which are involved in adipogenesis (Figure 5a). The induction of

those genes was not unexpected as *PPARγ* and several lipogenic genes are induced in the fatless mouse like $p53^{TSD/-}$ mice.[27] The induction of PPARγ-mediated programs might be a compensatory elevation of adipocyte differentiation against depleting fat.

We hypothesized that the induction of PPARγ-mediated differentiation in the skin of $p53^{TSD/-}$ mice affected SG differentiation. Blimp1$^+$ cells were initially reported as a progenitor cells for SG differentiation, but more recently as differentiating sebocytes.[8,28] Cells expressing Blimp1 in the SG were depleted in the whole skin sections of $p53^{TSD/-}$ mice and in the epidermal sheets of the $p53^{TSD/-}$ mouse tails (Figures 5b and c). This depletion was also shown in the *Puma$^{-/-}$* background. Consistently, cells stained with Blimp1 in the epidermis of $p53^{TSD/-}$ mice were decreased, compared with $p53^{+/-}$ mice (Figure 5d). Next, we tested whether or not PPARγ is involved in the depletion of Blimp1$^+$ cells by using the PPARγ antagonist, bisphenol A diglycidyl
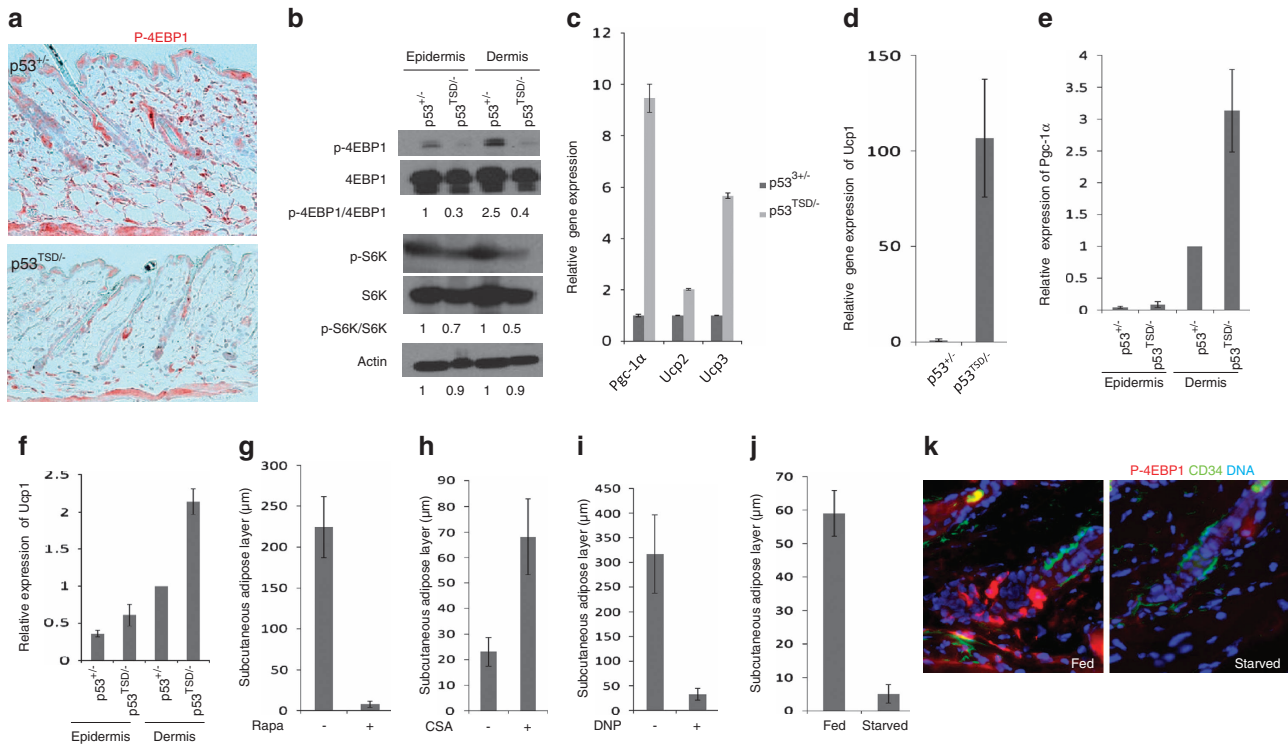
Figure 3 The reduction of subcutaneous adipose tissue in skin of p53$^{TSD/-}$ mice is correlated to the reduced mTORC1 activity and increased energy expenditure. (**a**) Phosphorylation of 4EBP1 in the skin of *p53*$^{TSD/-}$ mice was reduced when compared with that in *p53*$^{+/-}$ mice as determined by immunohistochemistry (IHC). (Magnification, × 50). (**b**) The phosphorylation of 4EBP1 and S6K was reduced in the skin of p53$^{TSD/-}$ mice when compared with that in *p53*$^{+/-}$ mice. Samples from epidermis and dermis/subcutaneous fat layer were analyzed by western blotting. (**c, d**) The relative expression of genes related to energy expenditure in the skin of *p53*$^{+/-}$ and p53$^{TSD/-}$ mice as determined by quantitative RT-PCR analysis. Values represent means ± S.D. *n* = 3. (**e, f**) The relative expression of *PGC-1α* and *Ucp1* in the skin of p53$^{+/-}$ and p53$^{TSD/-}$ mice as determined by quantitative RT-PCR analysis. Samples from epidermis and dermis/subcutaneous fat layer were analyzed. Values represent means ± S.D. *n* = 3. (**g**) The thickness of the subcutaneous fat layer in the skin of 5-week-old p53$^{TSD/-}$ Puma$^{-/-}$ mice treated with or without Rapa for 7 days. The data were derived from skin sections stained with H&E. (**h**) The thickness of the subcutaneous fat layer in the skin of 4-week-old p53$^{TSD/-}$ Puma$^{-/-}$ mice treated with or without CSA for 7 days. (**i**) The thickness of the subcutaneous fat layer of 4-week-old p53$^{+/-}$ mice treated with or without DNP for 7 days. (**j**) The thickness of the subcutaneous fat layer in the skin of starved and fed p53$^{+/-}$ mice. (**k**) Reduced phosphorylation of 4EBP1 in the skin of starved p53$^{+/-}$ mice. Phosphorylation of 4EBP (red) and CD34 (green) in the skin of starved and fed p53$^{+/-}$ mice were shown by IF (Magnification, × 100)

ether (BADGE). Indeed, the reduction of Blimp1^{+} cells in the SG of *p53*$^{TSD/-}$ mice was rescued by BADGE. These results demonstrate that PPARγ is involved in the depletion of Blimp1^{+} sebocytes in the skin of *p53*$^{TSD/-}$ mice. Moreover, in the old *p53*$^{TSD/-}$ mice in the *Puma*$^{-/-}$ background, it seemed that the SG at P180 essentially disappeared (Figures 5e and f). Notably, *p53*$^{TSD/-}$ *Puma*$^{-/-}$ mice had subcutaneous adipose tissues at P90 but not P180, suggesting that subcutaneous adipose tissues are correlated to SG depleted by p53 activation in the skin. In addition, the SG of *p53*$^{TSD/-}$ mice showed atrophy such as a reduction of the SG size and a decline in the number of cells (Figures 5g–i).

DNA damage foci, a reliable indicator of *in vivo* senescence, which was increased in the whole mount of tail skin from *p53*$^{TSD/-}$ mice, was partially rescued by BADGE, specifically in the SG but not in adjacent bulge or hair germ cells (Figures 6a and b). In addition, the expression of another senescence marker gene, p16, in the skin of *p53*$^{TSD/-}$ mice was normalized by BADGE treatment (Figures 6c and d). In contrast, the expression of p53 target genes, *PML* was not normalized by BAGE (Figure 6e). Metabolic genes such as *Srebp1*, *Scd1*, and *Glut4*,[29,30] which were upregulated in the skin of *p53*$^{TSD/-}$ mice, were normalized by BADGE

(Figure 6f). These results demonstrate that PPARγ-induced differentiation and the following depletion of progenitor cells are prerequisites to senescence occurring within the SG of *p53*$^{TSD/-}$ mice.

The antioxidant *N*-acetyl cysteine (NAC) could also ameliorate γ-H2A.X in the skin of *p53*$^{TSD/-}$ mice (Figure 6g). However, in contrast to BADGE, NAC reduced not only γ-H2A.X in the SG but also in the bulge in the skin of *p53*$^{TSD/-}$ mice (Figure 6g). This suggests that ROS induces senescence in the skin of *p53*$^{TSD/-}$ mice but not specifically in the SG. As ROS induces PPARγ-dependent differentiation of the adipocytes,[31] we checked whether NAC could also ameliorate the depletion of Blimp1^{+} in the SG of *p53*$^{TSD/-}$ mice. In contrast to BADGE, it was not rescued by NAC (Figure 6h). Therefore, our results indicate that activated p53 in the skin elevates PPARγ in the skin that may then lead to the depletion of sebocytes. In the skin of aged wild-type mice, the subcutaneous fat layers were consistently reduced when compared with the skin of young mice (Supplementary Figure S7a). In addition, PPARγ was increased in the skin of old mice (Supplementary Figure S7b). Although the reduction of the fat layers in the skin of old mice were not as much as depleted in the skin of p53-activated mice, this consistency supports the
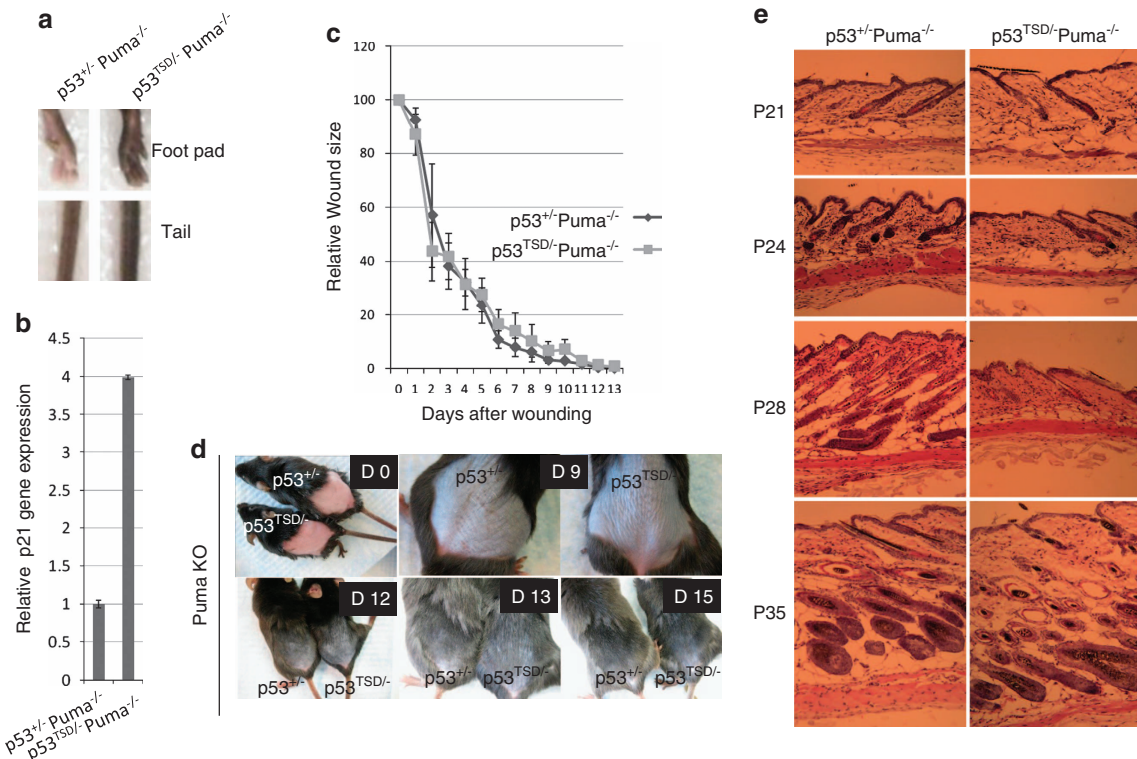
Figure 4 Hyperactivation of p53 in the skin slows hair cycle, but does not impact on either hair re-growth after shaving or closure after wounding. (**a**) Macroscopic appearance of tails and footpads of 4-week-old $p53^{+/-}Puma^{-/-}$ mice and $p53^{TSD/-}Puma^{-/-}$ mice. p53$^{TSD/-}$Puma$^{-/-}$ mice display hyperpigmentation. (**b**) The relative expression level of $p21$ in the skin of $p53^{+/-}Puma^{-/-}$ mice and $p53^{TSD/-}Puma^{-/-}$ mice was determined by quantitative RT-PCR analysis. $n=3$. Values represent means ± S.D. Wound heal assay (**c**) and hair re-growth assay (**d**) in the skin of 2-month-old $p53^{+/-}Puma^{-/-}$ mice and $p53^{TSD/-}Puma^{-/-}$ mice. Values represent means ± S.D. (**e**) H&E analyses in the skin of the $p53^{TSD/-}Puma^{-/-}$ mice or p53$^{+/-}$Puma$^{-/-}$ mice at P21, P24, P28, and P35. Data indicate that hair follicle cycle is delayed in p53-activated mouse

notion that the reduction of fat layers and the depletion of sebocytes, in which PPARγ was involved as observed in p53-activated mice, is correlated to the procedures of the normal skin aging. This conclusion is consistent with previous findings that PPARγ regulates cellular senescence by modulating p16 expression in the old fibroblasts.[32]

Discussion

In this study, the use of T21D and S23D mutations more specifically reflects DNA damaging stressors normally associated with skin aging such as DNA damage induced by exposure to the sun. In this model system, there was only a slight defect observed in epidermal structures of $p53^{TSD/-}$ mice, which showed slow hair follicle cycling, but normal hair growth and wound healing. However, dermal structures, poorly characterized in previous p53-dependent accelerated aging, showed the most dramatic defect with severe depletion of the subcutaneous adipose lipid stores. Despite using as an obvious marker of skin aging[3] and an important role in the control of the hair follicle cycle,[23] the mechanism underlying the loss of subcutaneous adipose during aging has been poorly understood. Here, we suggest that the decreased mTOR signaling in the subcutaneous fat of $p53^{TSD/-}$ mice is involved in the reduction of subcutaneous adipose, resulting in failure to maintain SG progenitor cells. We found that $p53^{TSD/-}$ mice displayed atrophy of the SG in the old age

similar to the inactivation of SG in older humans. As there is a specific depletion of Blimp1$^+$ cells in SG of $p53^{TSD/-}$ mice and the differentiation inducer PPARγ is increased, our results suggest the depletion of the progenitor pool through enhanced differentiation. The result that depleted Blimp1$^+$ cells in SG of $p53^{TSD/-}$ mice were normalized by treatment of PPARγ antagonist not only supported those ideas but also suggested the mechanism of senescence in the skin is by PPARγ-mediated differentiation (Figures 5 and 6). The increase of PPARγ activity in the skin of $p53^{TSD/-}$ mice might be attributed to the reduction of subcutaneous fat. In support of this notion, the induction of $PPAR\gamma$ and several lipogenic genes are induced in the fatless mouse like $p53^{TSD/-}$ mice, as a complementary pathway to induce adipogenesis.[27]

Interestingly, it was reported that p53 also inhibits hyper MYC-induced SG differentiation, although loss of p53 did not affect normal SG homeostasis.[28] In contrast to our observation that DNA damage response is not involved in PPARγ-dependent SG differentiation in p53-activated mice, DNA damage response is important for the inhibition of SG differentiation by p53 activation in the MYC-induced model. It suggests that the function of p53 on SG differentiation is correlated to how SG differentiation is induced and p53 is activated, for those may determine how much p53 is involved in the differentiation.

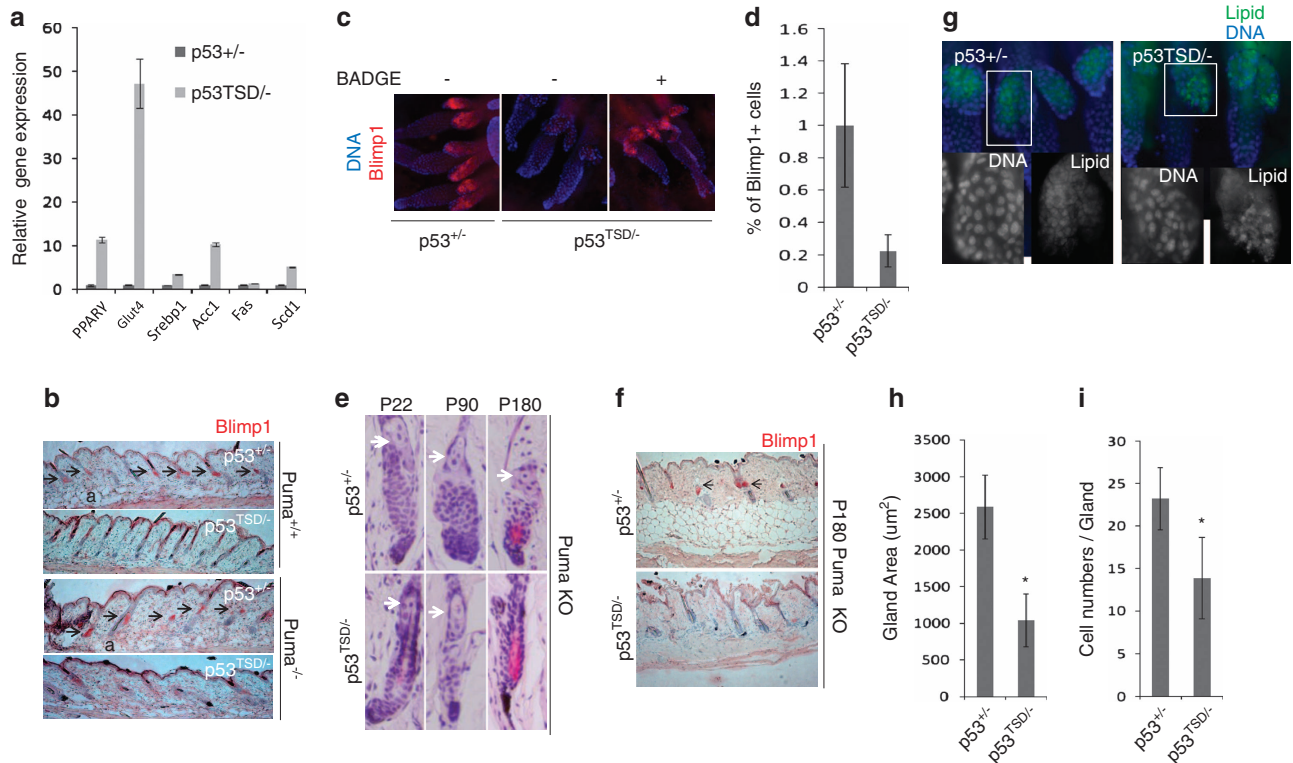Our findings indicate that the depletion of Blimp1$^+$ cells in SG and the atrophy of SG are correlated to reduction

Figure 5 The induction of PPARγ in *p53*[TSD/−] mice leads to the depletion of Blimp1^{+} progenitor of sebocyte. (**a**) The relative expression level of genes involved in adipogenesis in the skin of *p53*^{+/−} and *p53*[TSD/−] mice determined by quantitative RT-PCR analysis. *n* = 3. Values represent means ± S.D. (**b**) IHC for Blimp1 in the skin of *p53*[TSD/−] and *p53*^{+/−} mice. (Magnification, × 25). (**c**) Epidermal sheets of *p53*^{+/−}, *p53*[TSD/−], *p53*[TSD/−] *Puma*^{−/−} mice, and *p53*^{+/−} *Puma*^{−/−} mice with or without PPARγ antagonist BADGE were labeled for Blimp1 (red) as a sebocyte progenitor marker by IF (Magnification, × 50). (**d**) FACS analysis of Blimp1 cells in the skin of *p53*[TSD/−] mice. *n* = 3 from three mice for each genotype. Values represent means ± S.D. Cells expressing SG progenitor marker, Blimp1 reduced in the skin of *p53*[TSD/−] mice (**e**) H&E analyses in the skin of the *p53*[TSD/−] *Puma*^{−/−} mice and *p53*^{+/−} *Puma*^{−/−} mice at P24, P90, and P180. Data show that SG is rapidly depleted in *p53*[TSD/−] mice and this atrophy is correlated to the reduction of subcutaneous fat layer. Arrow, SG (Magnification, × 100). (**f**) IHC for Blimp1 in the skin of P180-old *p53*[TSD/−] *Puma*^{−/−} mice and *p53*^{+/−} *Puma*^{−/−} mice. Data show that Blimp1 cells are located in SG of *p53*^{+/−} mice, but depleted in *p53*[TSD/−] mice (Magnification, × 25). (**g–i**) Reduced size and cell number of SG in *p53*[TSD/−] mice. Epidermal sheets of *p53*^{+/−} and *p53*[TSD/−] mice were labeled with lipid dye Nile Red (green) and DAPI. After taking pictures of IF in the same scale, the area of SG was measured and cells in this area were counted with ImageJ; *n* equal over 100 cells from three mice for each genotype. Values represent means ± S.D. and *t*-test used to calculate the statistical significance, *P < 0.05. (Magnification, × 100)

of subcutaneous fat that might point out the importance for maintaining subcutaneous fat in the elderly. That is, if subcutaneous fat is properly maintained, healthy skin can be preserved by controlling SG that delivers lipids that contribute to affecting skin hydration and dryness.[7,33]

Materials and Methods

Animal experiments. All mice were bred and cared for as described previously under the supervision of the Institutional Animal Care and Use Committee (IACUC) at UCSD.[1]

Chemicals such as 2,4-dinitrophenol (DNP; 8 mg/kg, Sigma, St Louis, MO, USA), BADGE (80 mg/kg, Sigma), NAC (80 mg/kg, Sigma), and cyclosporine A (CSA; 60 mg/kg, LC Laboratories, Woburn, MA, USA) were injected to 3-week-old mice intraperitoneally (i. p.) every other day for 7 days. The final injection volume was adjusted to 50 μl with 0.9% sodium chloride. For starvation experiments, 3-week-old mice were deprived of food for 3 days with water.

Wound-healing assay and hair re-growth assay. For wound healing assay, full-thickness excisional skin wounds were created on the dorsum of 8-week-old mice with 5 mm biopsy punch. Wounds were photographed regularly and wound closure is calculated based on wound size relative to the original wound dimensions by the ImageJ software (National Institutes of Health, Bethesda, MD, USA). For hair re-growth assay, the hair on the dorsum of 8-week-old mice was removed by paraffin and the hair growth was monitored regularly.

Skin transplantation. Donor mice were 3-day-old *p53*^{+/−} and *p53*[TSD/−] mice. After killing, full-thickness skins were uniformly trimmed then transplanted onto prepared graft sites on the dorsum of the SCID mice. Dressings were removed under anesthesia after 1 week. The skin grafts were monitored by growing new hair and analyzed after 4 weeks.

Histological analysis. Histological analysis was performed as described.[1] Briefly, dorsal skins from euthanized 3–4-week-old mice were fixed in 10% buffered formalin for 24 h, transferred to 70% ethanol, embedded in paraffin, and sliced. The sections were stained with hematoxylin and eosin (H&E) for histological assessment.

For analyzing the thickness of each skin layers and adipocytes, dorsal skin sections from four mice for each genotype were stained with H&E, and at least three pictures were taken for each section in the same scale. The dermal region, the epidermal region, and subcutaneous adipose region were determined in the photomicrographs on the basis of their histological appearance, and then the length of each region were measured by measurement tool of the ImageJ software. Adipocytes were counted in the equal area of subcutaneous adipose region and more than 100 adipocytes were applied to ImageJ for the quantification of size.

For immunohistochemistry for either the phosphorylation of 4E-binding protein (4EBP)1 or Blimp1, general immunohistochemical procedures of UCSD Histology Core were applied to skin paraffin sections with anti p-4EBP1 antibody (Cell Signaling Technology, Danvers, MA, USA; 1: 50) and anti-Blimp1 antibody (Novus, Littleton, CO, USA or Santa Cruz Biotechnology, Santa Cruz, CA, USA; 1: 100), respectively.
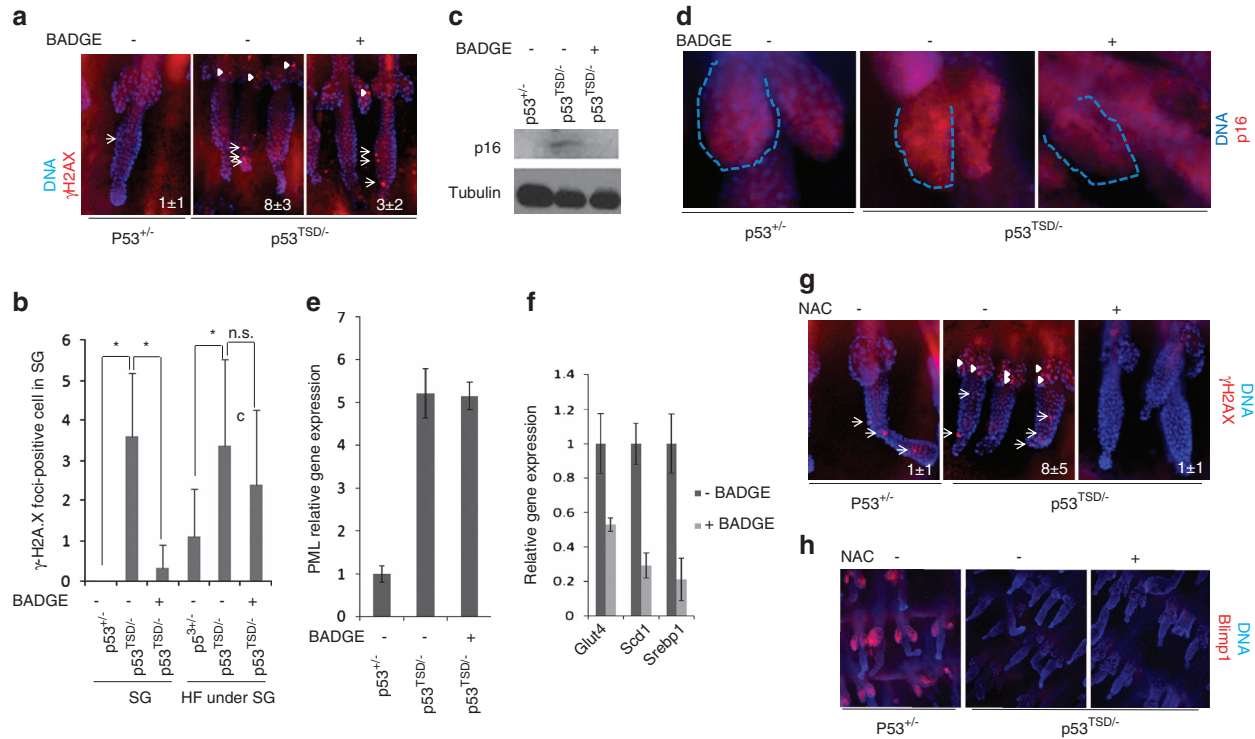
Figure 6 p53-induced senescence is related to PPARγ-dependent differentiation and ROS. (**a**) γ-H2A.X (red) in the epidermal sheets of $p53^{+/-}$ mice and $p53^{TSD/-}$ mice treated with or without BADGE is analysed by IF and representative images are shown. Total cells with DNA damage foci in the each HF are counted and shown in each panel (Magnification, × 100). (**b**) The increased number of cells with DNA damage foci in SG is rescued by BADGE. Epidermal sheets of $p53^{+/-}$ mice and $p53^{TSD/-}$ mice treated with or without BADGE were labeled for γ-H2A.X by IF and quantified by counting cells with DNA damage foci. $n = 30$–40 HF for each genotype. Values represent means ± S.D. and t-test was used to calculate the statistical significance, *$P < 0.05$; NS, not significant. Arrowheads indicate cells with DNA damage foci in the SG while arrows indicate cells with DNA damage foci in HF under SG. (**c**) Immunoblotting for p16 was performed after extracting proteins from the skin of $p53^{+/-}$ mice and $p53^{TSD/-}$ mice treated with or without BADGE. (**d**) Epidermal sheets of $p53^{+/-}$ and $p53^{TSD/-}$ mice treated with or without BADGE were labeled by IF for p16 (red) as a senescent marker. (**e**) The relative expression level of PML in the skin of $p53^{+/-}$ and $p53^{TSD}$ mice treated with or without BADGE was determined by quantitative RT-PCR analysis. $n = 3$. Values represent means ± S.D. (**f**) The relative expression level of genes involved in adipogenesis in the skin of $p53^{TSD}$ mice treated with or without BADGE were determined by quantitative RT-PCR analysis. $n = 3$. Values represent means ± S.D. (**g**) The increased number of cells with DNA damage foci in HF of $p53^{TSD/-}$ mice are normalized by NAC treatment. Epidermal sheets of $p53^{+/-}$ mice and $p53^{TSD/-}$ mice treated with or without NAC were labeled for γ-H2A.X (red) by IF and representative images are shown. Cells with DNA damage foci in each HF are counted. $n = 30$–40 HFs for each genotype. Values represent means ± S.D. and t-test was used to calculate the statistical significance, *$P < 0.05$ (Magnification, × 50). (**h**) Sebocyte progenitors depleted in $p53^{TSD/-}$ mice are not rescued by ROS chelating. Epidermal sheets of $p53^{+/-}$ mice or $p53^{TSD/-}$ mice treated with or without NAC were labeled for Blimp1 (red) as a sebocyte progenitor marker by IF (Magnification, × 25)

Fluorescence microscope. Frozen skin tissues were used for immunofluorescence (IF). The frozen tissues embedded in OCT were cryosectioned into 5 μm thickness and blocked in phosphate-buffered saline (PBS) with 2.5% goat serum for 30 min. For a hair follicle stem cells marker CD34, sections were incubated for 20 min with FITC-anti-CD34 antibody (RAM34 eBioscience, San Diego, CA, USA; 1: 50) in blocking solution at room temperature, washed three times with PBS, and mounted with VECTASHIELD (Vector Laboratories, Burlingame, CA, USA) mounting media containing 4,6-diamidino-2-phenylindole (DAPI). Images were acquired using an inverted epifluorescence microscope (AxioVision, Zeiss, Göttingen, Germany).

For assessing epidermal differentiation, mouse skin isolated from wild-type and genetically modified animals were frozen in OCT (Tissue-Tek, Sakura Finetek USA, Torrance, CA, USA). Staining for epidermal basal layer marker Keratin 5 and suprabasal layer maker Keratin 10 was performed on 8-μm frozen sections after the tissues were fixed for 10 min in 4% paraformaldehyde. Images were acquired on an Olympus Bx51 microscope with an Olympus DP70 camera. Acquisition was performed using a 40 × 1.3 UPlan FL N objective (Olympus).

For immunofluorescence assay of γ-H2A.X (Cell Signaling Technology) and Blimp1, the method for epidermal whole mounts was performed with a little modification as described.[34] Briefly, epidermal sheets were peeled out from skin pieces of mice tails incubated with 5 mM EDTA in PBS for 8 h. Epidermal sheets were fixed in 4% paraformaldehyde (PFA) for 3 h, permeabilized/blocked with 0.5% Triton X-100, 0.5% skimmed milk, 2.5% goat serum in PBS for 2 h. The epidermal sheets were applied overnight to primary antibodies in blocking buffer, washed three times for 2 h every washing step with 0.3% Tween 20 in PBS, and incubated with secondary antibodies conjugated with Alexa-Fluor 568 for 30 min. The epidermal sheets were rinsed in PBS and mounted with VECTASHIELD containing DAPI.

Lipid-containing cells staining. Whole mount lipid staining of fixed epidermal sheets were stained with Nile Red (100 ng/ml in PBS) for 10 min, washed with PBS, mounted with VECTASHIELD containing DAPI, and immunofluorescence of the epidermal sheet was performed as previously described.[34]

Senescence analysis. To analyze senescent cells in the skins, an immunofluorescent protocol using DNA damage foci and a cytochemical protocol, SA-β-Gal were performed. DNA damage foci were assessed by IF of γ-H2A.X on the epidermal sheets as described above. After images were acquired using an inverted epifluorescence microscope, cells with DNA damage foci in each HF were counted using ImageJ. SA-β-Gal assay was performed using cellular senescence assay kit as the manufacturer's instruction (Cell Signaling). The cryosections of skin were overnight fixed in 10% buffered formalin, washed three times in PBS, and stained with solutions to develop positive signal for 4 h at 37 °C. In the microphotocopies from more than three sections, hair follicles with positive signal were counted.

FACS analysis. FACS analysis of senescence was performed using Quantitative Cellular Senescence Assay Kit (Cell Biolabs, San Diego, CA, USA) as the manufacturer's protocol. Briefly, preparation of single cells from dorsal skin was through treating minced skin tissues with trypsin and collagenase followed by filtration using a 70 μm mesh filter. Cells were incubated with pretreatment solution at 37 °C for 2 h, subsequently applied to SA-β-Gal substrate solution at 37 °C for 4 h with gentle agitation. After washing stained cells three times with PBS, FACS analysis was performed in the PBS with 1% FBS on a LSRII flow cytometer (BD Bioscience, San Jose, CA, USA) and analyzed using FlowJo software (TreeStar, Ashland, OR, USA) as described.[1] For FACS analysis of Blimp1^{+} cells, after subcutis was removed with scalpel, epidermis was separated from mouse's dorsal skin by incubating overnight with trypsin. Epidermis was further processed to single cells by pipetting with trypsin and filtering through 40 μm mesh filter. For intracellular staining of Blimp1, fixation/permeabilization buffer (Assay Designs, Ann Arbor, MI, USA) and permeabilization wash buffer (Biolegend, San Diego, CA, USA) were used as the manufacturer's instruction. Staining with Blimp1 antibody was followed by staining with secondary antibodies conjugated with Alexa-Fluor 568.

Quantitative PCR. RNA extraction through real-time PCR analysis was performed as previously reported.[35] Total RNA was extracted from mice skins using Trizol (Invitrogen, Carlsbad, CA, USA) as the manufacturer's instructions and purified by RNAeasy Mini Kit (Qiagen, Valencia, CA, USA). For separating between epidermis and dermis/subcutaneous fat, dispase is used at 4 °C for O/N. One microgram of total RNA was reverse transcribed using high capacity cDNA reverse transcriptase kit (Applied Biosystems, Foster City, CA, USA). Real-time PCR was performed with an ABI Prism 7000 (Applied Biosystems) with FastStart Universal SYBR Green Master (Roche, Indianapolis, IN, USA). The PCR conditions were as follows: 10 min at 95 °C, 40 cycles of 15 s at 95 °C, and 1 min at 60 °C. The average Ct value for each gene was determined from triplicate reactions and normalized with the amount of β-actin. The sequence of primers used in this study will be provided on request.

Analysis of apoptotic cells in the skin sections. Apoptotic cells in the tissue sections were detected by terminal deoxyribonucleotide (TdT) transferase-mediated nick-end labeling (TUNEL) assay kit (BD Bioscience) as previously described, following manufacturer's instructions.[1] Briefly, deparaffinized tissue sections on the slides were incubated with proteinase K for 15 min and quenched in 0.3% hydrogen peroxide for 30 min. The sections were incubated in equilibration buffer for 10 min and applied to TdT (terminal deoxynucleotidyl transferase) enzyme solution for 1 h at 37 °C. After the slides were agitated for 15 s and incubated for 10 min at room temperature, those sections were incubated with the anti-digoxin antibody for 30 min at room temperature in a humidified chamber and developed by peroxidase substrate 3-amino-9-ethylcarbazole (AEC) (3-amino-9-ethylcarbazole; Vector Laboratories) for 15 min. The hematoxylin was used for counterstaining. Cells with positive signal in each hair follicle were counted from more than three photomicrographs of the skin sections labeled with TUNEL using ImageJ.

IF for active form of Caspase3 (active caspase3) was performed by using anti-cleaved Caspase3 antibody (Cell Signaling Technology) as another assessment of apoptosis following above IF protocol.

Western blotting. After separating epidermis and dermis, skin tissues were homogenized in the lysis buffer (150 mM NaCl, 1% NP-40, 0.5% sodium deoxycholate, 0.05% SDS (sodium dodecyl sulfate), 50 mM Tris pH 8.0, phosphatase inhibitor cocktail, protease inhibitor cocktail). Boiled samples with sample buffer were separated on 8–15% SDS polyacrylamide gel electrophoresis (PAGE), transferred to nitrocellulose membrane. The blots were blocked in blocking buffer (5% skim milk in PBS with 0.05% Tween 20), incubated with primary antibodies in the blocking buffer. After washing three times with blocking buffer, blots were probed with a horseradish peroxidase-conjugated secondary antibody and developed with Super signal West Dura (Thermo, Rockford, IL, USA). p-4EBP1 antibody, 4EBP1 antibody (Cell signaling, 9644P), S6K antibody (Cell signaling, 2708P), and p-S6K antibody (Cell signaling, 9205P) were used.

Conflict of Interest

The authors declare no conflict of interest.

Author contributions

JK and YX designed the experiments; JK executed the majority of experiments; MN and CJ are involved in data analysis and skin functional studies; DT, C-YY, and BL performed animal related experiments. JK, CJ, and YX were responsible for the initial draft of the manuscript while other authors contributed to the final edition.

1. Liu D, Ou L, Clemenson Jr GD, Chao C, Lutske ME, Zambetti GP et al. Puma is required for p53-induced depletion of adult stem cells. Nat Cell Biol 2010; 12: 993–998.
2. Gannon HS, Donehower LA, Lyle S, Jones SN. Mdm2-p53 signaling regulates epidermal stem cell senescence and premature aging phenotypes in mouse skin. Dev Biol 2011; 353: 1–9.
3. Baumann L. Skin ageing and its treatment. J Pathol 2007; 211: 241–251.
4. Tyner SD, Venkatachalam S, Choi J, Jones S, Ghebranious N, Igelmann H et al. p53 mutant mice that display early ageing-associated phenotypes. Nature 2002; 415: 45–53.
5. Jahoda CA, Christiano AM. Niche crosstalk: intercellular signals at the hair follicle. Cell 2011; 146: 678–681.
6. Blanpain C, Fuchs E. Epidermal homeostasis: a balancing act of stem cells in the skin. Nat Rev Mol Cell Biol 2009; 10: 207–217.
7. Fluhr JW, Mao-Qiang M, Brown BE, Wertz PW, Crumrine D, Sundberg JP et al. Glycerol regulates stratum corneum hydration in sebaceous gland deficient (asebia) mice. J Invest Dermatol 2003; 120: 728–737.
8. Horsley V, O'Carroll D, Tooze R, Ohinata Y, Saitou M, Obukhanych T et al. Blimp1 defines a progenitor population that governs cellular input to the sebaceous gland. Cell 2006; 126: 597–609.
9. Zouboulis CC, Boschnakow A. Chronological ageing and photoageing of the human sebaceous gland. Clin Exp Dermatol 2001; 26: 600–607.
10. Zouboulis CC, Adjaye J, Akamatsu H, Moe-Behrens G, Niemann C. Human skin stem cells and the ageing process. Exp Gerontol 2008; 43: 986–997.
11. Makrantonaki E, Adjaye J, Herwig R, Brink TC, Groth D, Hultschig C et al. Age-specific hormonal decline is accompanied by transcriptional changes in human sebocytes in vitro. Aging Cell 2006; 5: 331–344.
12. Elewa RM, Abdallah M, Youssef N, Zouboulis CC. Aging-related changes in cutaneous corticotropin-releasing hormone system reflect a defective neuroendocrine-stress response in aging. Rejuvenation Res 2012; 15: 366–373.
13. Makrantonaki E, Zouboulis CC. The skin as a mirror of the aging process in the human organism–state of the art and results of the aging research in the German National Genome Research Network 2 (NGFN-2). Exp Gerontol 2007; 42: 879–886.
14. Georgel P, Crozat K, Lauth X, Makrantonaki E, Seltmann H, Sovath S et al. A toll-like receptor 2-responsive lipid effector pathway protects mammals against skin infections with gram-positive bacteria. Infect Immun 2005; 73: 4512–4521.
15. Bouska A, Eischen CM. Murine double minute 2: p53-independent roads lead to genome instability or death. Trends Biochem Sci 2009; 34: 279–286.
16. Makrantonaki E, Schonknecht P, Hossini AM, Kaiser E, Katsouli MM, Adjaye J et al. Skin and brain age together: the role of hormones in the ageing process. Exp Gerontol 2010; 45: 801–813.
17. Cui R, Widlund HR, Feige E, Lin JY, Wilensky DL, Igras VE et al. Central role of p53 in the suntan response and pathologic hyperpigmentation. Cell 2007; 128: 853–864.
18. Wang C, Jurk D, Maddick M, Nelson G, Martin-Ruiz C, von Zglinicki T. DNA damage response and cellular senescence in tissues of aging mice. Aging Cell 2009; 8: 311–323.
19. Polak P, Cybulski N, Feige JN, Auwerx J, Ruegg MA, Hall MN. Adipose-specific knockout of raptor results in lean mice with enhanced mitochondrial respiration. Cell Metab 2008; 8: 399–410.
20. Tsukiyama-Kohara K, Poulin F, Kohara M, DeMaria CT, Cheng A, Wu Z et al. Adipose tissue reduction in mice lacking the translational inhibitor 4E-BP1. Nat Med 2001; 7: 1128–1132.
21. Budanov AV, Karin M. p53 target genes sestrin1 and sestrin2 connect genotoxic stress and mTOR signaling. Cell 2008; 134: 451–460.
22. Seale P, Conroe HM, Estall J, Kajimura S, Frontini A, Ishibashi J et al. Prdm16 determines the thermogenic program of subcutaneous white adipose tissue in mice. J Clin Invest 2011; 121: 96–105.
23. Festa E, Fretz J, Berry R, Schmidt B, Rodeheffer M, Horowitz M et al. Adipocyte lineage cells contribute to the skin stem cell niche to drive hair cycling. Cell 2011; 146: 761–771.
24. Rosenfield RL, Kentsis A, Deplewski D, Ciletti N. Rat preputial sebocyte differentiation involves peroxisome proliferator-activated receptors. J Invest Dermatol 1999; 112: 226–232.
25. Rosen ED, Sarraf P, Troy AE, Bradwin G, Moore K, Milstone DS et al. PPAR gamma is required for the differentiation of adipose tissue in vivo and in vitro. Mol Cell 1999; 4: 611–617.
26. Dozsa A, Dezso B, Toth BI, Bacsi A, Poliska S, Camera E et al. PPAR gamma-mediated and arachidonic acid-dependent signaling is involved in differentiation and lipid production of human sebocytes. J Invest Dermatol 2013; 15: 1–11.

27. Chao L, Marcus-Samuels B, Mason MM, Moitra J, Vinson C, Arioglu E *et al.* Adipose tissue is required for the antidiabetic, but not for the hypolipidemic, effect of thiazolidinediones. *J Clin Invest* 2000; **106**: 1221–1228.

28. Cottle DL, Kretzschmar K, Schweiger PJ, Quist SR, Gollnick HP, Natsuga K *et al.* c-MYC-induced sebaceous gland differentiation is controlled by an androgen receptor/p53 axis. *Cell Rep* 2013; **3**: 427–441.

29. Schwartzenberg-Bar-Yoseph F, Armoni M, Karnieli E. The tumor suppressor p53 down-regulates glucose transporters GLUT1 and GLUT4 gene expression. *Cancer Res* 2004; **64**: 2627–2633.

30. Yahagi N, Shimano H, Matsuzaka T, Najima Y, Sekiya M, Nakagawa Y *et al.* p53 activation in adipocytes of obese mice. *J Biol Chem* 2003; **278**: 25395–25400.

31. Tormos KV, Anso E, Hamanaka RB, Eisenbart J, Joseph J, Kalyanaraman B *et al.* Mitochondrial complex III ROS regulate adipocyte differentiation. *Cell Metab* 2011; **14**: 537–544.

32. Gan Q, Huang J, Zhou R, Niu J, Zhu X, Wang J *et al.* PPAR{gamma} accelerates cellular senescence by inducing p16INK4{alpha} expression in human diploid fibroblasts. *J Cell Sci* 2008; **121**(Pt 13): 2235–2245.

33. Sakuma TH, Maibach HI. Oily skin: an overview. *Skin Pharmacol Physiol* 2012; **25**: 227–235.

34. Braun KM, Niemann C, Jensen UB, Sundberg JP, Silva-Vargas V, Watt FM. Manipulation of stem cell proliferation and lineage commitment: visualisation of label-retaining cells in wholemounts of mouse epidermis. *Development* 2003; **130**: 5241–5255.

35. Song H, Chung SK, Xu Y. Modeling disease in human ESCs using an efficient BAC-based homologous recombination system. *Cell Stem Cell* 2010; **6**: 80–89.

Supplementary Information accompanies this paper on Cell Death and Disease website (http://www.nature.com/cddis)